BRAIN. Broad Research in Artificial Intelligence and Neuroscience
e-ISSN: 2067-3957 | p-ISSN: 2068-0473
Covered in: Web of Science (ESCI); EBSCO; JERIH PLUS (hkdir.no); IndexCopernicus; Google Scholar; SHERPA/RoMEO; ArticleReach Direct; WorldCat; CrossRef; Peeref; Bridge of Knowledge (mostwiedzy.pl); abcdindex.com; Editage; Ingenta Connect Publication; OALib; scite.ai; Scholar9; Scientific and Technical Information Portal; FID Move; ADVANCED SCIENCES INDEX (European Science Evaluation Centre, neredatatics.org); ivySCI; exaly.com; Journal Selector Tool (letpub.com); Citefactor.org; fatcat!; ZDB catalogue; Catalogue SUDOC (abes.fr); OpenAlex; Wikidata; The ISSN Portal; Socolar; KVK-Volltitel (kit.edu)
2025, Volume 16, Issue 4, pages: 406-423
Submitted: July 29th, 2025 | *Accepted for publication:* October 24th, 2025

Retrospective Histopathological Aspects in the Recurrence of Bladder Tumours Following TUR-B: Insights into Progression and Regression Patterns, Computational Aspects and the Relevance of AI

Bogdan Novac
Department of Urology, "Dr. C.I. Parhon" Hospital, Iași, Romania.
bogdannvc@gmail.com,
https://orcid.org/0000-0003-4501-1718

Alin Ciobica*
Department of Biology, Faculty of Biology, Alexandru Ioan Cuza University of Iași, Carol I Avenue, No. 20A, 700506, Iași, Romania; "Olga Necrasov "Center, Depart. Of Biomedical Research, Romanian Academy, Iași Branch, Teodor Codrescu Street 2, 700481, Iași, Romania.
Academy of Romanian Scientists, 3 Ilfov Street, 050044, Bucharest, Romania
"Ioan Haulică" Institute, Apollonia University, Păcurari Street 11, 700511, Iași, Romania. alin.ciobica@uaic.ro,
https://orcid.org/0000-0002-1750-6011

Radu Zara*
Department of Urology, "Dr. C.I. Parhon" Hospital, Iași, Romania.
zara.radu00@gmail.com,
https://orcid.org/0009-0003-6154-620X

Ion Chiriac
Department of Urology, "Dr. C.I. Parhon" Hospital, Iași, Romania.
ion.chiriak@gmail.com,
https://orcid.org/0009-0000-8422-0614

Abstract: ***Background:*** *Bladder cancer is one of the most common urological malignancies worldwide, often requiring multiple transurethral resections of the bladder (TUR-B) due to high recurrence rates. This* ***retrospective*** *study analyses* ***389 histopathological (HP) reports*** *from* ***117 patients*** *to evaluate the evolution of tumour grade (G1, G2, G3) and invasion level (non-invasive vs. invasive) in recurrent bladder tumors.* ***Methods:*** *We included patients who underwent two or more TUR-B interventions between 2009 and 2024, had complete HP data for each resection, and were followed to assess recurrence, progression, and regression. Descriptive statistics and chi-square tests were used to examine differences in tumour behaviour among subgroups. Endpoints included recurrence (any new tumour), progression (increase in grade or stage to ≥T2), stagnation (no change in grade or stage), and regression (downgrade or downstage from invasive to non-invasive).* ***Results:*** *Nearly 15% of non-invasive tumours progressed to invasive disease, whereas over 30% of tumours initially classified as invasive showed partial or complete regression during subsequent resections. G2 tumours were most prevalent (around 55%), with more than half exhibiting stagnation. Some high-grade (G3) lesions demonstrated notable regression rates, highlighting possible responsiveness to intravesical therapy.* ***Conclusions:*** *These findings underscore the heterogeneity of bladder tumour evolution following TUR-B and the importance of vigilant surveillance and adjuvant therapies. While a subset of invasive tumours may regress, others progress despite initial low-grade presentation. Future prospective or multivariate analyses are needed to identify precise predictors of progression and regression in non-muscle-invasive bladder cancer (NMIBC). Also considering our previous expertise in the connections with AI and both urology and cancer, this could open further discussions and relevance in this growing area of research.*

Keywords: artificial intelligence; machine learning; deep learning; bladder cancer; urothelial tumour; degree of malignancy; non-musculo-invasive; muscle invasive; cancer progression; cancer regression.

How to cite: Novac, B., Ciobica, A., Zara, R., Chiriac, I., Agachi, M., & Novac, O. (2025). Retrospective histopathological aspects in the recurrence of bladder Tumours following TUR-B: Insights into progression and regression patterns, computational aspects and the relevance of AI. *BRAIN. Broad Research in Artificial Intelligence and Neuroscience*, *16*(4), 406-423. https://doi.org/10.70594/brain/16.4/25

Marcel Agachi
Department of Urology, "Dr. C.I. Parhon" Hospital, Iași, Romania. marcel.agachi@gmail.com,
https://orcid.org/0009-0007-0878-4507

Otilia Novac
Department of Biology, Faculty of Biology, Alexandru Ioan Cuza University of Iași, Carol I;
Faculty of Medicine, University of Medicine and Pharmacy "Grigore T. Popa", 16 Universității Street, 700115, Iași, Romania. otilia76@gmail.com, https://orcid.org/0000-0002-4708-3603

* *Correspondence authors*

1. Introduction

Bladder cancer is one of the most common urological malignancies, ranking 10th globally in terms of cancer incidence. Approximately 573,000 new cases occur each year, with around 200,000 annual deaths. Men are disproportionately affected (approximately 3:1), and incidence increases with age, particularly after 65 years (Zhang et al., 2023; Babjuk et al., 2022). Bladder tumours are classified into muscle-invasive and non-muscle-invasive types, each with distinct implications for prognosis and management. Non-muscle-invasive bladder cancer (NMIBC) accounts for 75–85% of diagnoses and requires careful follow-up due to a high propensity for recurrence and progression (Quhal et al., 2021; Ferro et al., 2018). Transurethral resection of the bladder (TUR-B/TURBT) is considered the standard initial treatment for NMIBC, enabling both resection and histopathological evaluation (Compérat et al., 2019). However, a substantial proportion of patients experience tumour recurrence, sometimes with an increase in malignancy grade (e.g., G2 to G3) or upstaging from non-invasive (Ta/T1) to muscle-invasive disease (≥T2). By contrast, regression—defined as a decrease in tumour grade or a return from invasive to non-invasive status—may occasionally occur, potentially influenced by intravesical therapies such as Bacillus Calmette-Guérin (BCG) (Sylvester et al., 2006; Witjes et al., 2017). In this retrospective study, we examined 117 patients with recurrent bladder tumours who underwent multiple TUR-B procedures between 2009 and 2024. Our primary aim was to characterise the patterns of progression, stagnation, and regression across repeated resections, offering new insights into bladder tumour dynamics that may inform personalised treatment strategies for NMIBC.

2. Materials and Methods

Study Design and Inclusion Criteria

We conducted a retrospective cohort analysis of patients treated at our institution for urothelial bladder tumours from 2009 to 2024.

Eligible patients met the following criteria:

- At least two TUR-B procedures performed for tumour recurrence;
- Complete histopathological data (G1, G2, or G3; non-invasive vs. invasive) for each resection;
- Adequate follow-up to monitor recurrence, progression, or regression.
- Patients with non-urothelial tumours, incomplete pathology reports, or only palliative resections were excluded. Severe comorbidities directly influencing bladder cancer prognosis also served as grounds for exclusion.

The study was approved by the Ethics Committee of "Dr. C.I. Parhon" Clinical Hospital in Iași.

Definitions

Recurrence: Any new histologically confirmed tumour after a prior TUR-B.

Progression: An increase in malignancy grade (e.g., G1→G2 or G2→G3) or a shift from non-invasive (Ta/T1) to muscle-invasive (≥T2).

Stagnation: Recurrence without any change in grade or stage.

Regression: A decrease in grade (e.g., G3→G2/G1) or a return from muscle-invasive to non-muscle-invasive disease.

All histopathological assessments were carried out by experienced pathologists, though variations in WHO classification schemes and interpretive differences may have arisen during the 15-year period.

Data Collection

We retrospectively reviewed clinical records, surgical reports, and pathology results. Variables included patient age, sex, comorbidities, and any intravesical therapies administered (e.g., chemotherapy, BCG). Because of the extended timescale, data completeness varied, which could introduce bias. We documented these limitations in a dedicated section below.

Statistical Analysis

We utilised descriptive statistics (frequencies, percentages) to report distributions of grade and invasion status. Chi-square tests were performed to determine statistical significance ($p < 0.05$) for differences in progression or regression rates among subgroups (G1 vs. G2 vs. G3, non-invasive vs. invasive).

The chi-square analyses were performed using the total number of anatomopathological (AP) resections, with each report treated as an independent observation. The analysis was therefore conducted at the resection-episode level rather than the patient level, as the aim was to evaluate the distribution of tumour grades and stages across successive procedures.

Owing to retrospective data constraints, no formal multivariate analysis was undertaken, though future prospective work might incorporate logistic regression or Cox proportional hazards models.

This approach more accurately captures the temporal dynamics of tumour evolution.

3. Results

3.1. Patient and Tumour Characteristics

A total of 117 patients were included in our retrospective analysis, yielding 389 anatomopathological (AP) reports. The mean age of the cohort was 70.36 years (SD = 8.64), with 82 (70.1%) being male and 35 (29.9%) female. Data on comorbidities and intravesical therapies were incomplete or unavailable, preventing further correlation of these factors with tumour evolution. Sixteen patients presented with carcinoma in situ (CIS), though incomplete follow-up details limited more specific analyses regarding its prognostic impact.

Table 1. Distribution of Tumours by Malignancy Grade and Invasion Status

Malignancy Grade	Non-invasive n(%)	Invasive n(%)	No tumour (n)	Total (n)	p-value*
G1 (n=4)	4 (100.0)	0 (0.0)	–	4	–
G2 (n=216)	160 (74.1)	56 (25.9)	–	216	0.031
G3 (n=137)	70 (51.1)	67 (48.9)	–	137	0.041
Non-tumoural (n=32)	–	–	32	32	–
Total (n=389)	234	123	32	389	–

Notes:
Non-invasive = Ta/T1; *Invasive* = ≥T2.
"No tumour" indicates negative histopathological findings (e.g., no residual tumour tissue).
p-value* columns represent example results from Chi-square tests comparing the distribution between non-invasive and invasive across grades (G2 vs. G3).

Table 1 presents the overall distribution of tumour grade (G1, G2, G3) and invasion status (non-invasive vs. invasive), along with the subset of specimens that displayed no residual tumour on pathological examination ("no tumour"). Among the 389 total AP reports, 4 corresponded to G1 tumours, 216 to G2 tumours, and 137 to G3 tumours, whereas 32 showed no tumour. Of the 389 specimens, 234 (60.2%) were classified as non-invasive (Ta/T1), and 123 (31.6%) were invasive (≥T2). In 32 samples (8.2%), no neoplastic tissue was identified. In this dataset, G2 tumours constituted the largest subset (55.5% of all AP reports). G3 lesions accounted for 35.2%, while G1 tumours represented 1.0%.

The non-tumoral category represented 8.2%. Based on chi-square testing, the p-values indicated statistically significant differences in the distribution of non-invasive versus invasive tumours when comparing G2 to G3, but no inferential statistics were performed beyond these initial tests. Specific p-values are displayed in the corresponding table.

3.2. Malignancy Grade Evolution

Progression, Stagnation, and Regression in Grade

We next examined how the malignancy grade shifted across repeated TUR-B resections (e.g., G1 → G2/G3, G2 → G3 for progression; no change for stagnation; or G3 → G2/G1 for regression). The percentages of each phenomenon are summarised in Table 2. They represent the proportion of cases showing progression, stagnation, or regression within each tumour grade category (G1, G2, G3). Consequently, the values are not expected to sum to 100% across each row, as each percentage is calculated strictly within its grade-specific subgroup, not across all cases. The absolute numbers presented in the text (62, 169, 46) are derived directly from the dataset and correspond precisely to the distributions observed for each grade category. The table reflects analyses performed per resection episode, rather than per patient, which explains the perceived discrepancies when comparing percentages to patient counts.

Table 2. Percentage Distribution of Progression, Stagnation, and Regression in Malignancy Grade

Malignancy Grade	Progression (%)	Stagnation (%)	Regression (%)
G1 (n=4)	75.0	0.0	0.0
G2 (n=216)	18.52	55.55	6.48
G3 (n=137)	0.0	32.11	23.36

Progression malignancy grade: A total of 62 cases demonstrated an increase in tumour grade, defined here as G1 → G2/G3 or G2 → G3. Among G1 tumours (n=4), 3 instances proceeded to a higher grade, whereas 18.52% of the G2 subset progressed to G3.

Stagnation in malignancy grade: Grade stagnation was noted in 169 cases (43.4%), where sequential resections did not reveal any change in grade compared to the prior pathological diagnosis. Of these, a substantial fraction were G2 (n=120), while G3 lesions accounted for 44 stagnant cases over time.

Regression in malignancy grade: Regression of malignancy grade, characterised by a G3 → G2/G1 or G2 → G1 shift, occurred in 46 cases (11.8%). The majority of these regressions originated from the G3 subset (23.36% of G3 tumours) and, to a lesser extent, from G2 lesions (6.48% of G2). Situations in which G1 tumours decreased further in grade were not observed, given that G1 is already classified as the lowest grade included in this analysis.

3.3. Invasion Grade Evolution

3.3.1. Baseline Ratio of Non-invasive vs. Invasive Tumours

At the time of each TUR-B, 234 pathology samples were characterised as non-invasive (Ta/T1), and 123 were classified as invasive (≥T2). The remaining 32 samples displayed no tumour. Evaluating changes in invasion status across repeated interventions allows for an assessment of upstaging (Ta/T1 → ≥T2), no change in invasion category, or downstaging (≥T2 → Ta/T1).

3.3.2. Progression, Stagnation, and Regression in Invasion

Table 3. Percentage Distribution of Progression, Stagnation, and Regression in Invasion Grade

Invasion Grade	**Progression (%)**	**Stagnation (%)**	**Regression (%)**
Total non-invasive (n=234)	14.95	68.80	–
Total invasive (n=123)	–	32.52	34.14
Non-invasive **G1** (n=4)	0.0	75.0	–
Non-invasive **G2** (n=160)	16.88	65.63	–
Non-invasive **G3** (n=70)	5.71	47.14	–
Invasive **G2** (n=56)	–	28.57	50.0
Invasive **G3** (n=67)	–	35.82	20.90

Progression of invasion status: Out of 234 non-invasive tumour samples, 35 (14.95%) progressed to invasive stages at subsequent resections. The G2 subgroup had the highest numeric count of progression among non-invasive lesions, with 27 moving to a T2 or higher classification, whereas G3 non-invasive tumours accounted for 4 progressions.

Stagnation of invasion grade: In 161 (68.80%) of non-invasive tumours, the invasion status remained unchanged between TUR-B procedures. Specifically, 3 G1, 105 G2, and 33 G3 lesions (all initially classified as non-invasive) demonstrated no further increase in stage across subsequent resections. Meanwhile, 40 of the originally invasive tumours (32.52% of the invasive subset) did not show any upward stage migration at follow-up TUR-B.

Regression of invasion grade: Regression of invasion status was documented in 42 cases, representing 34.14% of the initially invasive tumours. Invasive G2 tumours underwent a shift to non-invasive in 28 instances (50% of such cases), whereas invasive G3 tumours demonstrated regression in 14 out of 67 cases (20.90%).

3.4. Carcinoma in situ (CIS) Subset

Sixteen patients were identified with a histopathological diagnosis of CIS in at least one TUR-B procedure. Because of incomplete data on clinical follow-up and therapy, no discrete analysis was undertaken to quantify changes in grade or invasion specifically attributable to CIS. No additional breakdown of recurrences or progressions within this subgroup was performed due to missing variables regarding therapy protocols and confirmatory biopsies.

4. Discussion

The present study underscores the dynamic and multifaceted nature of bladder cancer evolution when managed via transurethral resection of the bladder (TUR-B). Our updated dataset—comprising 117 patients with 389 anatomopathological (AP) reports—illustrates several key themes in non-muscle-invasive bladder cancer (NMIBC) and muscle-invasive disease. Notably, G2 tumours were the most prevalent, and a significant fraction of G3 lesions demonstrated both progression and regression in grade or invasion status. These findings are consistent with prior literature (Sylvester et al., 2006; van Rhijn et al., 2009), which emphasises the need for vigilant surveillance and repeated resections.

A substantial fraction of G2 lesions showed **stagnation** in malignancy grade across follow-up TUR-Bs, in line with reports suggesting that many intermediate-grade tumours remain stable but still carry a risk of eventual progression (Witjes et al., 2017; van Rhijn et al., 2009). However, the fact that approximately 18.52% of G2 lesions progressed to G3 aligns with known estimates of 10–20% progression in NMIBC (Sylvester et al., 2006; Cambier et al., 2016). This dichotomy—some tumours remaining stable while others progress—reiterates the longstanding concept that intermediate-grade urothelial carcinomas can follow diverse clinical trajectories (Witjes et al., 2017). It also highlights why consistent cystoscopic monitoring and timely resection of recurrent lesions are critical (Babjuk et al., 2022).

From an invasion standpoint, approximately 15% of non-invasive tumours progressed to muscle-invasive disease (≥T2). This observation supports earlier work indicating that superficially appearing lesions (Ta/T1) can adopt more aggressive phenotypes over time (Compérat et al., 2019). Of particular interest, we also documented a notable regression rate among invasive tumours—especially those initially categorised as invasive G2 (50% regression). These findings mirror other series reporting downstaging with comprehensive surgical margins and rigorous follow-up cystoscopies (Herr, 2001). Although the mechanism behind invasion grade regression remains incompletely understood, it may involve a combination of adequate surgical technique, the biological heterogeneity of tumours, and the immunological or chemotherapeutic environment (Malmström et al., 2009).

Multiple studies have demonstrated that Bacillus Calmette-Guérin (BCG) instillations, coupled with thorough surgical resection, can effectively lower the risk of progression in NMIBC (Witjes et al., 2017; Malmström et al., 2009; Schulze et al., 2007). In particular, high-grade tumours (G3) often benefit from adjuvant intravesical therapy (Malmström et al., 2009). Although a subset of high-grade (G3) lesions in our cohort displayed regression, we were unable to fully assess the impact of intravesical therapy because such treatments were performed externally and not documented in our institutional records. This challenge of incomplete treatment logs is a known obstacle in retrospective analyses (Sylvester et al., 2006). Future studies with robust data on BCG protocols and other immunomodulatory approaches could elucidate how these interventions specifically influence regression rates in both G2 and G3 tumours.

We identified **16 patients** with a histopathological diagnosis of **carcinoma in situ (CIS)**, a known risk factor for recurrence and progression in bladder cancer (Naspro et al., 2022; McFadden et al., 2024). While CIS often correlates with worse outcomes, incomplete follow-up details impeded a conclusive evaluation of how CIS affected tumour behaviour in our cohort. Additionally, the **incomplete comorbidity data** restricted our ability to assess how coexisting conditions might influence disease trajectories or tolerance to treatment. Future prospective or multicentre investigations, with robust data collection, could illuminate whether patients with specific comorbidities or CIS subtypes might require more intensive surveillance or a different therapeutic approach.

Beyond simple dichotomies of progression vs. stability, our observations of **grade and invasion regression**—especially in G3 or muscle-invasive tumours—reflect growing evidence that certain tumour subtypes respond favourably to **immunomodulatory** or **chemotherapeutic** interventions (Herr, 2001; Malmström et al., 2009). In standard clinical practice, however, these regression events remain relatively rare, reported in fewer than 10–15% of high-grade recurrent cases in some series (Millán-Rodríguez et al., 2000). Here, the variable success of resection and possible immunotherapy highlight the **heterogeneity** of bladder cancer, where patient-specific or tumour-specific factors likely drive divergent outcomes.

Our study's retrospective design, spanning 15 years, introduces inherent challenges: **missing records** on comorbidities and intravesical therapies, variations in pathological assessment, and evolving WHO classification systems. Thus, while we report detailed findings on tumour grade and invasion changes, the incomplete nature of certain data elements (e.g., exact BCG protocols, comorbidity profiles) limits our ability to correlate these factors with observed regressions or progressions. Moreover, the presence of **16 CIS patients** further highlights the need for **standardised follow-up**—CIS can significantly alter risk stratification, yet its impact here remains undercharacterised due to insufficient clinical details.

Going forward, **multicentre prospective studies** with standardised data collection are warranted to confirm and expand upon our observations. Such investigations could better delineate which patients might undergo regression vs. progression and elucidate how immunotherapeutic or chemotherapeutic agents specifically mediate these outcomes (Malmström et al., 2009; Shariat et al., 2006). They could also clarify the implications of CIS, comorbidity burdens, and repeated TUR-B strategies in shaping long-term bladder cancer control.

5. Summary of Key Findings

Prevalence of High-Grade Tumours: A large proportion of G2 and G3 lesions was observed, consistent with advanced disease severity in many patients (Sylvester et al., 2006).

Frequent Grade Changes: About 16% of G2 tumours progressed to G3, while nearly 12% of all lesions underwent regression in grade—emphasising the dynamic nature of NMIBC (Malmström et al., 2009).

Notable Invasion Shifts: Approximately 15% of non-invasive tumours progressed, whereas ~34% of invasive tumours regressed, highlighting the potential efficacy of repeated resections and possibly adjuvant therapies (though data on the latter is lacking).

Missing Comorbidity and Therapy Data: Key variables (intravesical treatment records, comorbidities) could not be analysed, reducing our ability to correlate these factors with tumour evolution.

CIS Uncertainty: Sixteen CIS cases were identified, but incomplete follow-up data prevented a thorough assessment of its prognostic role.

These results collectively underscore the heterogeneity of bladder tumour evolution and reaffirm the importance of thorough pathological evaluation, repeated TUR-B, and effective documentation of adjuvant treatments (Babjuk et al., 2022; Compérat et al., 2019).

6. Limitations

Single-Centre Retrospective Design:

Conducted over a 15-year span, this study is subject to variability in pathology practices and potential selection bias. The use of multiple WHO classification systems during this period may further affect consistency.

Incomplete Comorbidity Data:

Although we aimed to assess the role of coexisting conditions (e.g., hypertension, diabetes), these details were insufficiently documented, limiting our ability to analyse how comorbidities might influence tumour behaviour or outcomes.

Lack of Intravesical Therapy Records:

Data on procedures such as Bacillus Calmette-Guérin (BCG) instillations were unavailable because they were performed at a separate institution that did not provide comprehensive treatment logs, reducing our capacity to correlate adjuvant therapies with recurrence or progression rates.

Partial Information on Carcinoma in situ (CIS):

Sixteen patients had a histopathological diagnosis of CIS, but incomplete clinical follow-up precluded a thorough evaluation of its impact on prognosis or long-term outcomes.

Heterogeneity of the Dataset:

Variations in reporting standards, patient follow-up intervals, and laboratory methods challenge the generalisability of these findings. Prospective or multicentre studies, ideally with standardised data collection, may yield more definitive insights into the roles of comorbidities, intravesical interventions, and CIS in bladder cancer evolution.

Moreover, taking into account our previous expertise at the intersection of artificial intelligence, urology, and oncology (Novac et al., 2024; Moroșan et al., 2024), the present findings have the potential to catalyse broader discussions and to enhance the scientific relevance of this work within an increasingly prominent and rapidly evolving research landscape.

7. Integrating AI into Bladder Cancer Diagnostics and Prognostics: A Review of Contemporary Models

7.1. Multi-Institutional Assessment of AI-Based Systems for Urothelial Neoplasm Classification in Digital Pathology

The following study presents a deep learning-based method for identifying normal, non-invasive, and invasive urothelial neoplasms using digitised histopathological images. Although there are numerous artificial intelligence (AI) models dedicated to cancer diagnosis, few focus on bladder lesions or clearly differentiate these essential categories. In this context, both convolutional neural networks (CNNs) and transformer models were developed and trained on a set of 12,500

whole-slide images (WSIs) from five institutions. Initial processing included normalisation of staining and partitioning of images into patches.

A five-fold cross-validation procedure was applied for the evaluation, using labels established by specialists. Among all the models analysed, EfficientNet-B6 stood out for its best performance, recording an accuracy of 0.913 (95% confidence interval, 0.907–0.920), a sensitivity of 0.909 (95% CI, 0.904–0.914), a specificity of 0.956 (95% CI, 0.953–0.960), an F1 score of 0.906 (95% CI, 0.901–0.911) and an AUC value of 0.983 (95% CI, 0.982–0.984). The obtained performances confirm the effectiveness and robustness of artificial intelligence-based methods in bladder cancer classification.

Although microscopic analysis of pathological slides is the basis of the diagnostic process, it is laborious, time-consuming, and can produce significant inter-specialist variation. In the context of a high case volume, repeated examinations can cause fatigue and increase the risk of errors, especially when differentiating structures with very similar morphological appearances, such as normal urothelium, non-invasive urothelial neoplasia, and invasive urothelial carcinoma. To overcome these limitations, artificial intelligence (AI) and deep learning techniques have become intensively explored topics due to their ability to improve diagnostic accuracy and efficiency in digital pathology.

This study aimed to develop a comprehensive histopathological model of the urinary bladder, one that would go beyond the limitations of biopsies or TUR-B specimens, which are primarily tumour-focused and limited to the mucosa and submucosa. By using data collected from multiple institutions, it was aimed to obtain a model that was as generalisable as possible and applicable to various clinical settings. The approach integrated a broad range of histological types—from normal tissue to non-invasive urothelial neoplasia to invasive urothelial carcinoma—and fully captured the anatomical structure of the urinary bladder, including the urothelium, lamina propria, muscularis propria (detrusor muscle), and adjacent stroma. Based on these data, a deep learning model was built, trained on diverse datasets, including radical cystectomy specimens, capable of classifying whole-slide images (WSI) into three major categories: normal, non-invasive urothelial neoplasia, and invasive urothelial carcinoma. The model demonstrated stability and good adaptive capacity, offering real potential to assist pathologists in formulating accurate diagnoses and supporting clinical decision-making.

The study included 12,500 whole-slide images (WSI), of which 1,500 were normal bladder tissue, 5,500 were non-invasive urothelial neoplasms, and another 5,500 were invasive urothelial neoplasias. Images classified as invasive urothelial carcinoma came from patients whose tumours infiltrated various anatomical structures: lamina propria (pT1: 2,575 cases, 46.82%), muscularis propria (pT2: 1,751 cases, 31.84%), perivesical soft tissue (pT3: 799 cases, 14.53%), and extravesical structures (pT4: 375 cases, 6.81%), respectively.

Most of the WSIs classified as non-invasive urothelial neoplasms originated from patients diagnosed with non-invasive papillary urothelial carcinoma (pTa, 4,728 cases; 85.96%) or urothelial carcinoma in situ (pTis, 712 cases; 12.95%). A very small percentage of this category derived from non-invasive components identified within invasive urothelial carcinomas (58 cases from pT1—1.05%, one case from pT2 and pT3—0.02% each, and no case from pT4).

In this study, the performance of four deep learning models was analysed using 5-fold cross-validation to assess how well they could differentiate between normal tissue, non-invasive lesions, and invasive lesions.

Of all the models tested, EfficientNet-B6 performed best. Although its sensitivity for the non-invasive category was 0.28% lower than that of DenseNet-121, the model outperformed DenseNet-121 by 1–2% in the other two classes, giving it the best overall performance.

After combining the confusion matrices from each fold into a single final matrix, EfficientNet-B6 continued to outperform. Even with a slight decrease in sensitivity in the non-invasive class compared to DenseNet-121, it demonstrated a consistent 1–2% advantage in the normal and invasive categories and outperformed ResNet-50 and ViT in all classes analysed.

As shown in Figure 1, the EfficientNet-B6 and DenseNet-121 models consistently highlighted large, pathologically relevant areas that matched features commonly used in diagnostic evaluation. ResNet-50 was also able to identify appropriate regions, but unlike the first two models, it focused on very narrow, point-like areas, risking losing important architectural information needed for correct classification.

In contrast, ViT generated scattered activations, frequently marking areas that did not correspond to the analysed classes or even empty portions of the image, which highlighted its limited pathological utility. In the case of non-invasive lesions, all three CNN-based models predominantly highlighted the tumor border—a central diagnostic landmark in pathological practice—while in invasive lesions, activations were distributed over larger tumor surfaces, without a well-defined main area.

Overall, DenseNet-121 and EfficientNet-B6 provided the most coherent and interpretable CAM patterns, followed by ResNet-50, while ViT ranked last in terms of relevance and consistency of activations (Park et al., 2025).

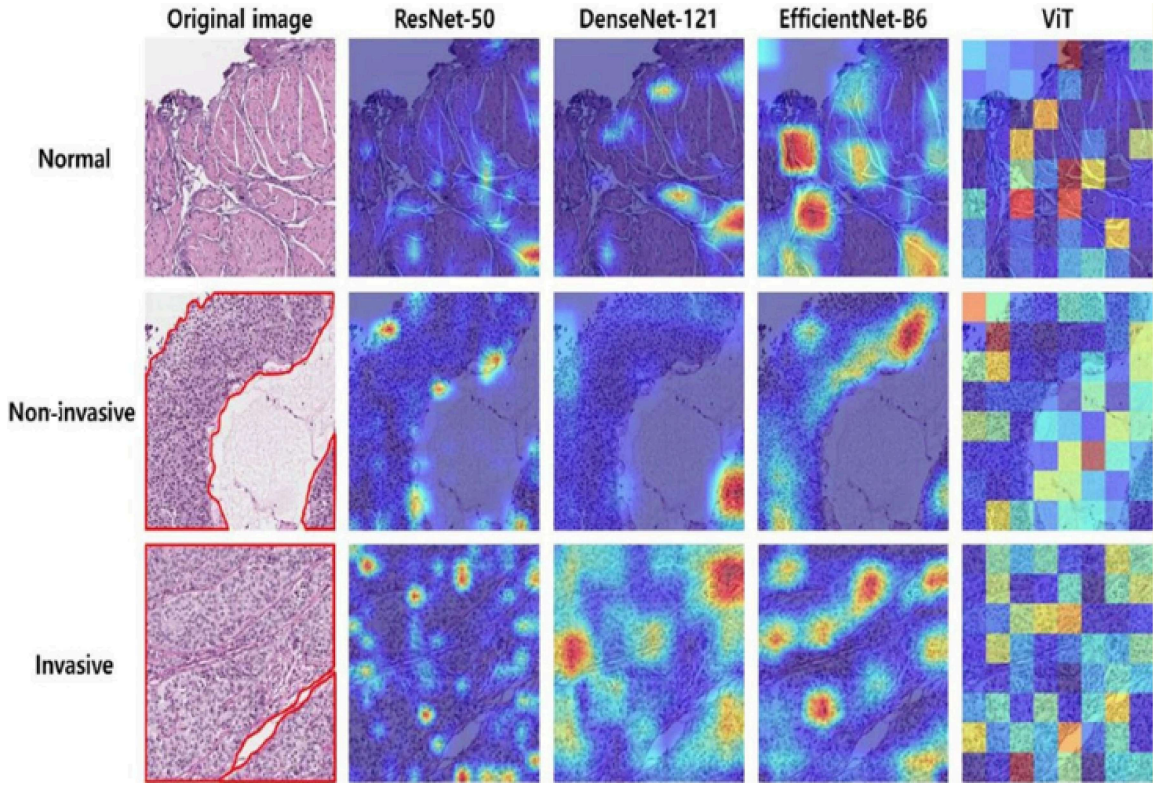

Figure 1. CAM visualisation results of ResNet-50, DenseNet-121, EfficientNet-B6, and ViT models. Source: Park, J. Y., Kim, J., Kim, Y. J., Kim, S. H., An, C. S., Kim, K. G., & Jung, C. K. (2025). Multi-institutional validation of AI models for classifying urothelial neoplasms in digital pathology. Scientific Reports, 15, 37215. https://doi.org/10.1038/s41598-025-21096-1Park, J. Y., Kim, J., Kim, Y. J., Kim, S. H., An, C. S., Kim, K. G., & Jung, C. K. (2025). Multi-institutional validation of AI models for classifying urothelial neoplasms in digital pathology. Scientific Reports, 15, 37215. https://doi.org/10.1038/s41598-025-21096-1

7.2. An Artificial Intelligence Model for the Pathological Diagnosis of Invasion Depth and Histologic Grade in Bladder Cancer

In recent years, with the increase in computation power and the increasing access to whole-slide images (WSI), artificial intelligence has made remarkable progress in many fields, especially in histopathological diagnosis. By analysing digital images, AI can identify subvisual details that are not perceptible to pathologists with direct examination, thus contributing to both

diagnosis and prognosis estimation. Numerous AI-based diagnostic systems have been developed, which have provided encouraging results in clinical applications. In particular, AI has proved to be extremely effective in interpreting biopsy specimens—often fragmented, reduced in quantity, or lacking contextual tissue—suggesting significant potential for the evaluation of lower-quality samples.

This study presents an artificial intelligence-based pathological diagnosis model (PAIDM) dedicated to bladder cancer (BCa). This model not only demonstrated remarkable accuracy in detecting muscle invasion, but also achieved robust results in histological grade classification, both at the patch and whole-slide image (WSI) levels. In addition, the performance of PAIDM was evaluated by directly comparing it with the diagnostic accuracy of pathologists.

In this study, 716 consecutive patients diagnosed with bladder cancer (BCa) at Sun Yat-sen Memorial Hospital (SYSMH), Sun Yat-sen University were analysed. All patients underwent transurethral resection of bladder tumour (TUR-B) between January 2013 and November 2019 and had histopathological confirmation of BCa, accompanied by complete clinical and pathological information.

The study group included both patients at the first diagnosis and patients who had previously received Bacillus Calmette-Guérin treatment or intravesical chemotherapy.

H and E-stained pathological slides of each case were collected and digitised as WSI images at 40× magnification using an automated scanner. Images of inadequate quality—either due to marked discoloration or poor resolution—as well as those that simultaneously showed low-grade and high-grade tumour cells in the same section were eliminated from the analysis.

Therefore, at the WSI image level, all cases were divided into three categories: high-grade muscle invasion (HGMI), high-grade non-invasive (HGNMI), and low-grade non-invasive (LGNMI).

For images with full annotations, there were additionally defined six types of patch-level labels: HGMI, HGNMI, LGNMI, unclear/unreadable area (IA), normal interstitial area (NIA), and noise/artefact area (NA). The HGMI category included both high-grade tumour cells and bladder muscle fibres, while HGNMI contained only high-grade tumour cells and LGNMI only low-grade tumours. The label IA designated the unclear regions caused by the scanning process, NIA referred to normal mesenchymal components, and NA indicated areas without cells, generated by staining artefacts.

The PAIDM model was built on the ScanNet deep learning algorithm. To differentiate the subtypes of bladder cancer — HGMI, HGNMI, and LGNMI —a convolutional neural network (CNN) derived from ScanNet, designed to provide fast results, compatible with current clinical practice. The training set, consisting of 393 images, was divided into two subsets: 318 images served to effectively train the PAIDM model, and 75 images were used to adjust the hyperparameters and refine the model's performance.

In the training phase, the six patch categories were loaded via dataloader, based on the txt file previously generated in the preprocessing step, and the patch-level classifier was trained using these data.

In the validation phase, the entire images were divided into patches, which were then fed into the CNN model to obtain the corresponding predictions. The individual patch results were subsequently reassembled to build heatmaps.

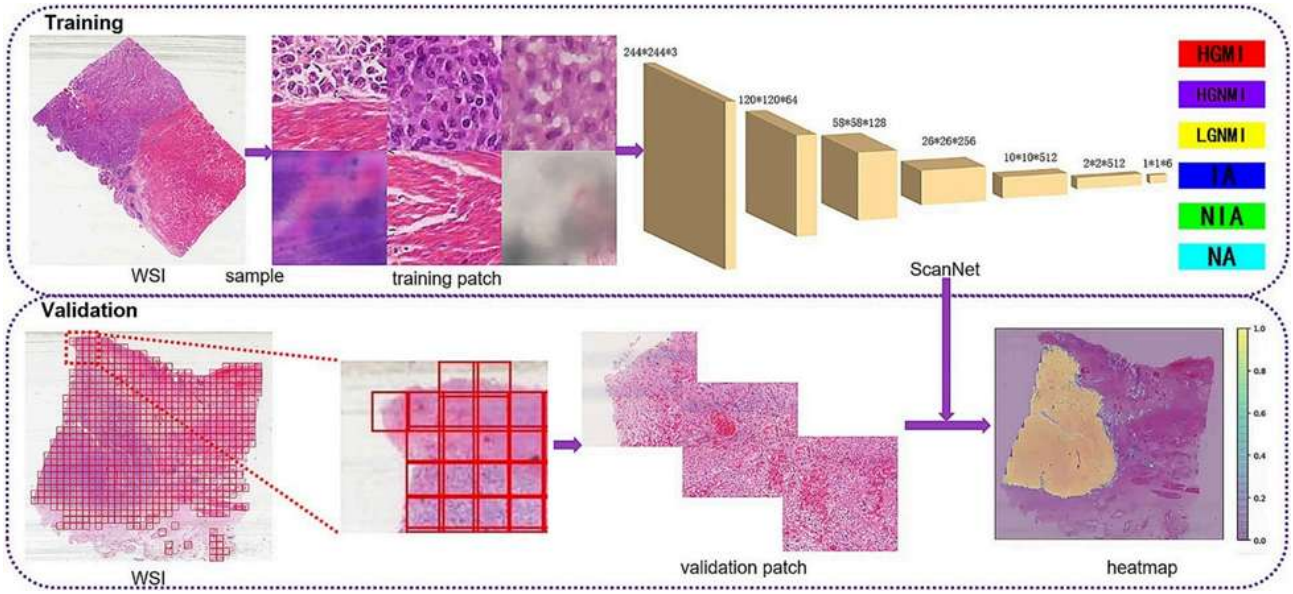

Figure 2. Schematic representation of the development and validation process for the pathology-based AI diagnostic model. Source: Pan, J., Hong, G., Zeng, H., Liao, C., Li, H., Yao, Y., Gan, Q., Wang, Y., Wu, S., & Lin, T. (2023). An artificial intelligence model for the pathological diagnosis of invasion depth and histologic grade in bladder cancer. Journal of Translational Medicine, 21, 42. https://doi.org/10.1186/s12967-023-03888-z

After obtaining the predictions, a six-channel heatmap was reconstructed, with each point representing the classification result of a patch. For each point, the final class was determined by selecting the channel with the maximum probability.

These heatmaps were then used to generate contours corresponding to each category, for which both the area and the mean probability were recorded, as shown in Figure 2. Finally, based on these values, appropriate formulas were applied to calculate the confidence level of the WSI-level classification for each class individually.

In all datasets analysed, the number of male patients greatly exceeded the number of female patients, with a male-to-female ratio of nearly 4:1. This distribution follows the well-known trend that bladder cancer occurs much more frequently in men. The NMIBC category includes stages Ta and T1, while MIBC includes lesions from T2 onwards. Approximately 70% of the cases were classified as NMIBC and approximately 30% as MIBC, proportions similar to those reported in the literature. It was also observed that high-grade tumours were more numerous than low-grade tumours.

The PAIDM model not only demonstrated outstanding performance in detecting muscle-invasive bladder carcinoma (MIBC), but also proved effective in differentiating high-grade from low-grade bladder tumours. Importantly, the model achieved robust results in both WSI and patch-level analysis, which gives it considerable potential for use in bladder cancer staging and grading.

The PAIDM model demonstrated good performance in detecting muscle invasion in WSI images, achieving an accuracy of 0.850 and a specificity of 0.941. However, its sensitivity was lower, reaching a value of 0.743. This decrease could be explained by the fact that some samples did not have a complete muscle layer, which prevented the model from extracting enough relevant features and led to the omission of some MIBC cases. It is important to emphasise that PAIDM also performed robustly at the patch level, where it recorded an AUC of 0.904, suggesting significant clinical potential for the evaluation of specimens with limited tissue.

In the comparative evaluation between PAIDM and pathologists, the model performed at least as well as the average of specialists, achieving the accuracy characteristic of an expert with

intermediate experience. This result indicates that PAIDM has the potential to increase the diagnostic accuracy of pathologists at the beginning of their careers or with a lower level of experience (Pan et al., 2023).

7.3. Deep Learning-Based Model for Prediction of Early Recurrence and Therapy Response on Whole Slide Images in Non-Muscle Invasive Bladder Cancer: A Retrospective, Multicentre Study

Over the past decade, artificial intelligence has shown remarkable potential in both diagnosing and predicting tumour progression. Various models based on machine learning algorithms have been developed to predict recurrence in NMIBC, but their effectiveness varies significantly depending on the populations analysed. Deep learning appears as a superior solution due to its ability to handle complex non-linear relationships and its stability when applied to large data sets.

In this study, an early recurrence prediction model (ERPM) was created for NMIBC patients. The performance of the ERPM was compared with that of traditional models, evaluating its ability to stratify recurrence-free survival (RFS). The potential of the model to predict the response of NMIBC patients to BCG therapy was also investigated.

This retrospective, multicentre study included consecutive patients diagnosed with NMIBC from five hospitals, covering the period January 1, 2017 – September 30, 2023. Eligibility criteria included: (1) TUR-B followed by immediate postoperative chemotherapy; (2) confirmation of NMIBC diagnosis by histopathological examination; (3)complete availability of clinicopathological data; (4) availability of H&E stained slides, with or without additional IHC stained slides.

The standard follow-up protocol for patients was cystoscopy and urinary cytology every 3–6 months for the first 2 years, then every 6 months for the next 3 years, and annually thereafter. Recurrence was confirmed histopathologically by the identification of bladder cancer in specimens obtained at TUR-B or cystectomy performed at least 3 months after the initial procedure. Tumour recurrence within the first 3 months was considered to represent a residual component of the original lesion.

Early recurrence was defined as disease recurrence within 2 years, given that intravesical therapy may have a delayed effect on reducing the risk of recurrence. Recurrence-free survival (RFS) was defined as the time from the time of TUR-B to the occurrence of recurrence, last follow-up visit, radical cystectomy, or death without recurrence.

The development of the ERPM model was structured in three successive steps. In the first step, the WSI images were fragmented into valid patches, and then a pre-trained feature extraction model was used to obtain the features corresponding to each patch. Subsequently, all the features extracted from the same case were brought together, depending on the type of data available (H&E only or H&E together with IHC).

The ERPM model is an ensemble system, consisting of two distinct sub-models. The selection of hyperparameters was performed through a combined approach, including both manual adjustments and automatic optimisation by the Neural Network Intelligence platform, using the Tree-structured Parzen Estimator strategy. The two submodels were configured with different sets of hyperparameters and were selected following two separate 5-fold cross-validation procedures.

In the last step, the pooled feature set for each case was fed into both submodels, generating both the bag-level and patch-level prediction confidence scores. Subsequently, the confidence value associated with the best-ranked patch (top 1) was combined by averaging with the bag-level prediction confidence score, thus obtaining the final result of each submodel. The final prediction of the case was calculated as the average of the two results provided by the component submodels.

The H&E image-based model used the same network architecture as the ERPM, with the only difference being the datasets used in the training and validation stages. This model was based exclusively on features extracted from H&E stained WSIs.The selection of variables included in the clinical model and the integrated model was performed using LASSO (Least Absolute Shrinkage

and Selection Operator) regression. To evaluate and compare the performance of the four models, ROC curves, decision curve analysis (DCA), and calibration curves were used.

Based on the ERPM model structure, a model for predicting treatment response (TRPM) was developed. For this purpose, patients with no prior BCG exposure who received intravesical BCG therapy in the SYSMH were included (the same patients used in the training cohort and the internal ERPM validation cohort).

According to the criteria established by the Food and Drug Administration (FDA),26 BCG-refractory NMIBC is defined as: persistent presence or recurrence of CIS within 12 months after completion of adequate BCG therapy;recurrence of Ta/T1 high-grade carcinoma within 6 months after completion of adequate BCG therapy; identification of T1 high-grade carcinoma at the first evaluation after BCG induction.

Adequate BCG therapy was defined as the administration of at least five of the six doses of the initial induction regimen, along with a minimum of two additional doses in the maintenance regimen or completion of a second induction regimen. Endpoints were defined as the occurrence of confirmed BCG-refractory NMIBC or the completion of the last follow-up visit at least 12 months after completion of adequate BCG therapy. Patients who did not meet these end points were excluded from the analysis. The TRPM training procedure followed the steps and logic also used in the development of the ERPM model.

In the internal validation cohort, ERPM achieved the highest AUC value (0.837; 95% CI: 0.757–0.918), significantly outperforming both the clinical and H&E-based models (DeLong test: $p < 0.0001$ and $p < 0.01$, respectively).

Decision curve analysis (DCA) revealed that ERPM provided a clear advantage over the other models across most threshold probability ranges. In each cohort, the differences between the ERPM and the integrated model did not reach statistical significance.

To further examine the prognostic value of ERPM, patients were divided into two categories—"high risk" and "low risk"—based on the classification generated by the model (in the training cohort: 322 vs. 250 patients; in the internal validation cohort: 87 vs. 46; and in the external validation cohorts: 287 vs. 283). Kaplan–Meier analysis performed for each cohort showed that patients in the high-risk group had significantly shorter recurrence-free survival (RFS) intervals compared with those in the low-risk group.

Based on univariate and multivariate Cox analyses performed in the training cohort, T stage (T1), histological grade (high grade), and previous recurrence were identified as relevant variables for building clinical and integrated Cox models.

In the validation cohorts, ERPM demonstrated significantly higher C-index values than the clinical Cox model and the H&E staining model (0.715–0.80 vs. 0.596–0.714, $p < 0.05$; 0.715–0.80 vs. 0.654–0.717, $p < 0.001$, respectively). At the same time, no significant differences were observed between ERPM and the integrated Cox model.

To assess the clinical applicability of the model, its ability to predict recurrence-free survival (RFS) across the various EAU-defined risk categories in the validation cohorts was evaluated. The results indicate that ERPM can significantly distinguish the level of recurrence risk within each EAU risk group.

To evaluate whether the ERPM structure can be adapted to predict patients who do not respond to intravesical BCG therapy, a derived model, called TRPM, was built using the ERPM architecture as a basis. 271 BCG-treated patients from the SYSMH cohort were included in the analysis. Following the 5-fold validation procedure, the model achieved an accuracy of 84.1%, a sensitivity of 69.0%, and a specificity of 88.3% (Jiang et al., 2025).

7.4. Evaluation of the Diagnostic Efficacy of the AI-Based Software INF-M01 in Detecting Suspicious Areas of Bladder Cancer Using Cystoscopy Images

The use of artificial intelligence in the diagnosis of bladder cancer has become an area of intense interest, as various AI applications have demonstrated the ability to identify, stage, and

assess tumour grade based on images from computed tomography (CT), magnetic resonance imaging (MRI), Haematoxylin–Eosin stained slides, or urinary cytology. Also, numerous studies have analysed the accuracy of AI in interpreting cystoscopy images for the diagnosis of bladder cancer, most of which reported very good results. In this direction, starting from a previous study, an artificial intelligence-based software was developed — INF-M01, version 1.0.0 — capable of automatically identifying the contours of potentially tumourous areas in cystoscopic images. The subsequent clinical study aimed to evaluate the performance of INF-M01, which automatically processes cystoscopy images and highlights regions suspicious for bladder cancer.

This study was designed as a retrospective, randomised, confirmatory clinical trial. The analysis examined cystoscopy images from patients who underwent this procedure to distinguish between bladder tumours and other suspicious bladder conditions. For the normal group, the inclusion criteria were as follows: (1) men undergoing cystoscopy to assess response to treatment for benign prostatic hyperplasia; (2) women undergoing cystoscopy for urinary tract symptoms; (3) patients undergoing cystoscopy to elucidate the cause of microscopic haematuria. Regarding the cancer group, the inclusion criteria were:(1) patients with suspected bladder tumours on imaging (ultrasound/CT/MRI), subsequently confirmed by biopsy performed after cystoscopy; (2) patients with a previous diagnosis of bladder cancer, who underwent cystoscopy as part of the follow-up monitoring and in whom the post-procedure biopsy reconfirmed the presence of the tumour.

The process of developing the reference standard involved extracting relevant frames from DICOM files containing endoscopic images, processing them, and uploading them to a specialised labelling platform. Urologists then analysed each image and applied labels based on the presence or absence of a tumour. Based on these labels, the images were then sorted into separate folders for cases confirmed as cancerous and those considered normal. This workflow was designed to ensure the accuracy and consistency of the reference standard used in the research.

The cystoscopy images were then assigned unique serial identifiers, and the interpretation results were recorded alongside a set of randomly generated numbers using the random shuffle method in Python. Randomisation was an essential step in maintaining the independence and objectivity of the analysed data, ensuring that both the AI-assisted assessment and the expert interpretation were performed on a set of images presented in a random order.

In this clinical study, five sets of images were created, randomly ordered and named A, B, C, D, and E. These sets were provided to the four participating clinicians, who used an artificial intelligence-assisted diagnostic software designed to identify bladder tumours. The analysis structure was as follows: set A was examined exclusively using INF-M01, an AI program specialised in cystoscopic image analysis, and the predictive results generated for each image were scored individually. This set served to evaluate the autonomous performance of the AI in detecting bladder tumours. For sets B–E, the image evaluation was performed by both the AI system and the four urologists. In these cases, the task was to identify the presence or absence of suspicious areas of bladder cancer and to delimit these suspicious regions.

Of the 1404 images classified as normal, 1293 were correctly recognised as free of lesions. The values of sensitivity, specificity, accuracy and confidence intervals (95% CI), calculated by the Wald method with continuity correction, were 0.973 (0.955–0.984), 0.921 (0.906–0.934) and 0.934 (0.922–0.945). The average Dice coefficient obtained was 0.903 (range 0.891–0.914). The reported performances exceed the sensitivity of 93.6% and specificity of 89.2%, indicating that INF-M01 was able to achieve the proposed level of accuracy in detecting areas suspicious for bladder cancer.

The mean Dice coefficient obtained by urologists ranged from 0.903 to 0.963, while the corresponding AI values ranged from 0.873 to 0.927. Among urologists, sensitivity, specificity, and accuracy ranged from 0.777 to 0.995, 0.984 to 0.996, and 0.931 to 0.991, respectively. For the AI system, sensitivity ranged from 0.952 to 0.977, specificity from 0.882 to 0.962, and accuracy from 0.904 to 0.959. Both the accuracy and mean Dice coefficient values were similar between the expert and AI assessments. These results suggest that artificial intelligence, such as urologists, is capable

of autonomously identifying and interpreting areas suspicious for bladder cancer in cystoscopy images, maintaining a high level of diagnostic performance (Kim et al., 2024).

7.5. Clinical Use of Machine Learning-Based Pathomics Signature for Diagnosis and Survival Prediction of Bladder Cancer

As an emerging technology with considerable potential, machine learning is increasingly being applied in medical image analysis for various types of malignant tumours, such as breast cancer, lung adenocarcinoma, neuro-oncology tumours, and skin carcinoma. However, the direct application of machine learning methods on pathological images has not yet been exhaustively explored in the case of bladder cancer (BCa). In this context, based on a machine learning algorithm, automated pathological models have been developed and validated, intended both for establishing the diagnosis and estimating the clinical prognosis in patients with bladder cancer.

This study included 108 patients diagnosed with bladder cancer (BCa) who underwent radical or partial cystectomy at Shanghai General Hospital between January 2009 and December 2016. The criteria used for patient selection were as follows: (a) confirmation of a primary malignant bladder tumour, accompanied by relevant clinicopathological information; (b) absence of other concomitantly diagnosed neoplasms; (c) availability of formalin-fixed paraffin-embedded (FFPE) tumour tissue samples from the patients. In addition, 406 BCa patients who met the first two inclusion criteria and for whom images of malignant histopathological sections were available in The Cancer Genome Atlas (TCGA) database were added. This group constituted the TCGA cohort used in the analysis.

The 108 FFPE specimens from patients with bladder cancer were sectioned into 5 μm slices, from which histological preparations were subsequently stained with haematoxylin and eosin. All H&E-stained slides were rigorously evaluated by an experienced pathologist specialising in genitourinary tract pathology. A Leica DM2500 LED fluorescence microscope was used to identify the area of interest, and the most representative image was selected from each specimen based on characteristics such as nuclear pleomorphism, mitotic activity, carcinoma infiltration, degree of tumour invasion, level of cellular differentiation, and overall histopathological grading. These elements reflect how a pathologist captures, in a single image, the essential aspects necessary for establishing the diagnosis.

A complete image processing workflow was developed for segmentation and feature extraction using different modules of the CellProfiler platform. First, the H&E-stained images were deconvoluted at a resolution of 1000 × 1000 pixels using the “UnmixColors” module. Subsequently, the images thus obtained were automatically segmented using the “IdentifyPrimaryObjects” and “IdentifySecondaryObjects” modules, which allowed the identification of cell nuclei and cytoplasm, respectively. In the next step, quantitative features related to the shape, size, texture and pixel intensity distribution were extracted using several analysis modules, including “Object Intensity Distribution”, “Object Intensity”, “Texture” and “Object Size Shape”. After excluding features considered unnecessary or redundant, 345 quantitative features were finally selected, which were used in subsequent analyses.

To develop the machine learning-based diagnostic model for bladder cancer (BCa) patients, H&E images from 406 BCa cases and 37 matched normal bladder tissue samples from TCGA were randomised divided into two independent sets—one for training and one for testing—in a 1:1 ratio, using a random seed generated in R. In addition, a batch of 108 BCa images and 53 normal bladder tissue images from Shanghai General Hospital was used as an external validation cohort to confirm the robustness and accuracy of the diagnostic model.

Based on the 345 quantitative features extracted for each H&E image in the training cohort, the glmnet11 package was used to perform LASSO (least absolute shrinkage and selection operator) analysis. This analysis allowed the identification of relevant digital factors for BCa and the determination of their weighted coefficients, on the basis of which the machine learning-based

diagnostic model was built. The final model was subsequently evaluated in both the test cohort and the external validation cohort.

To develop a clinical prognostic model for patients with bladder cancer (BCa), a LASSO–Cox hazard12 model was constructed using digital pathological images of the 406 patients included in the TCGA cohort (training cohort) to identify imaging features that correlated with survival. In addition, a risk score generated by machine learning methods was developed to provide the prognostic model with increased flexibility and predictive capacity.

By applying LASSO analysis accompanied by a 10-fold validation, 22 imaging factors relevant to bladder cancer (BCa) were selected.The automated segmentation highlighted clear differences between BCa tumour tissue and normal bladder tissue. At the same time, the machine learning-based diagnostic model demonstrated a very good discrimination capacity between BCa samples and normal samples, obtaining AUC values of 96.3%, 89.2% and 94.1% in the training, testing and external validation cohorts, which reflects a high diagnostic accuracy.

The model was subsequently evaluated in the differential diagnosis between BCa and glandular cystitis. The analysis revealed distinct differences in the objects identified between the two types of samples. The machine learning model was able to distinguish BCa patients from those with glandular cystitis with high accuracy, reaching an AUC value of 93.4%. When comparing BCa samples to all non-BCa samples (including normal tissue and glandular cystitis), the model still demonstrated excellent accuracy in identifying BCa cases, with an AUC value of 93.8%.

Overall survival analysis revealed significant differences between patients classified as high-risk and low-risk in the TCGA cohort (HR = 2.09, 95% CI: 1.56–2.81, P < .0001). The strong relationship between risk score and clinical outcome of bladder cancer was subsequently confirmed in an independent cohort. In the General cohort, survival differences between the two risk groups were also marked (HR = 5.32, 95% CI: 2.95–9.59, P < .0001), highlighting the utility of machine learning-based risk scoring in predicting the prognosis of patients with BCa.

Univariate and multivariate Cox analyses demonstrated that the machine learning-derived risk score was an independent predictor of survival in the TCGA cohort, a finding also validated in the General cohort. Furthermore, patients with BCa in advanced tumour stages (III/IV) had significantly higher risk score values. It was also observed that patients with high-grade tumours had higher risk scores compared to those with low-grade tumours (Chen et al., 2021).

8. Conclusions

In conclusion, our revised analyses reinforce that bladder tumour evolution following TUR-B (TURBT) can take multiple trajectories: from stagnation to significant progression, or even unexpected regression in certain subgroups. High-grade tumours, while aggressive, may exhibit variable therapeutic responses, potentially aided by re-resection and intravesical therapies. Nevertheless, incomplete comorbidity and adjuvant therapy data remain a significant barrier to fully understanding how external factors shape these outcomes. As the interplay between tumour biology, patient factors, and therapeutic interventions continues to be unraveled, careful attention to standardised data reporting and long-term follow-up will be essential for refining NMIBC management and improving patient prognoses.

References

Babjuk, M., Burger, M., Capoun, O., Cohen, D., Compérat, E. M., Dominguez Escrig, J. L., Gontero, P., Liedberg, F., Masson-Lecomte, A., Mostafid, A. H., Palou, J., van Rhijn, B. W. G., Rouprêt, M., Shariat, S. F., Seisen, T., Soukup, V., & Sylvester, R. J. (2022). European Association of Urology guidelines on non–muscle-invasive bladder cancer (Ta, T1, and carcinoma in situ). *European Urology, 81*(1), 75–94. https://doi.org/10.1016/j.eururo.2021.08.010

Cambier, S., Sylvester, R. J., Collette, L., Gontero, P., Brausi, M. A., van Andel, G., Kirkels, W. J., Silva, F. C., Oosterlinck, W., Prescott, S., Kirkali, Z., Powell, P. H., de Reijke, T. M.,

Turkeri, L., Collette, S., & Oddens, J. (2016). EORTC nomograms and risk groups for predicting recurrence, progression, and disease-specific and overall survival in non–muscle-invasive stage Ta–T1 urothelial bladder cancer patients treated with 1–3 years of maintenance Bacillus Calmette-Guérin. *European Urology, 69*(1), 60–69. https://doi.org/10.1016/j.eururo.2015.06.045

Chen, S., Jiang, L., Zheng, X., Shao, J., Wang, T., Zhang, E., Gao, F., Wang, X., & Zheng, J. (2021). Clinical use of machine learning-based pathomics signature for diagnosis and survival prediction of bladder cancer. *Cancer science*, *112*(7), 2905–2914. https://doi.org/10.1111/cas.14927

Compérat, E. M., Burger, M., Gontero, P., Mostafid, A. H., Palou, J., Rouprêt, M., van Rhijn, B. W. G., Shariat, S. F., Sylvester, R. J., Zigeuner, R., & Babjuk, M. (2019). Grading of urothelial carcinoma and the new "World Health Organisation classification of tumours of the urinary system and male genital organs 2016." *European Urology Focus, 5*(3), 457–466. https://doi.org/10.1016/j.euf.2018.01.003

Ferro, M., Vartolomei, M. D., Cantiello, F., Lucarelli, G., Di Stasi, S. M., Hurle, R., … & Shariat, S. F. (2018). High-grade T1 on re-transurethral resection after initial high-grade T1 confers worse oncological outcomes: Results of a multi-institutional study. *Urologia Internationalis, 101*(1), 7–15. https://doi.org/10.1159/000490765

Herr, H. W. (2001). Transurethral resection of muscle-invasive bladder cancer: 10-year outcome. *Journal of Clinical Oncology, 19*(1), 89–93. https://doi.org/10.1200/JCO.2001.19.1.89

Jiang, F., Hong, G., Zeng, H., Lin, Z., Liu, Y., Xu, A., Shen, R., Xie, Y., Luo, Y., Wang, Y., Zhu, M., Yang, H., Wang, H., Huang, S., Chen, R., Lin, T., & Wu, S. (2025). Deep learning-based model for prediction of early recurrence and therapy response on whole slide images in non-muscle-invasive bladder cancer: A retrospective, multicentre study. *eClinicalMedicine, 81*, 103125. https://doi.org/10.1016/j.eclinm.2025.103125

Kim, J., Ham, W. S., Koo, K. C., Lee, J., Ahn, H. K., Jeong, J. Y., Baek, S. Y., Lee, S. J., & Lee, K. S. (2024). Evaluation of the diagnostic efficacy of the AI-based software INF-M01 in detecting suspicious areas of bladder cancer using cystoscopy images. *Journal of Clinical Medicine*, 13(23), 7110. https://doi.org/10.3390/jcm13237110

Malmström, P. U., Sylvester, R. J., Crawford, D. E., Friedrich, M., Krege, S., Rintala, E., Solsona, E., Di Stasi, S. M., & Witjes, J. A. (2009). An individual patient data meta-analysis of the long-term outcome of randomised studies comparing intravesical mitomycin C versus bacillus Calmette-Guérin for non–muscle-invasive bladder cancer. *European Urology, 56*(2), 247–256. https://doi.org/10.1016/j.eururo.2009.04.038

McFadden, J., Tachibana, I., Adra, N., Collins, K., Cary, C., Koch, M., Kaimakliotis, H., Masterson, T. A., & Rice, K. R. (2024). Impact of variant histology on upstaging and survival in patients with non–muscle-invasive bladder cancer undergoing radical cystectomy. *Urologic Oncology, 42*(3), 69.e11–69.e16. https://doi.org/10.1016/j.urolonc.2023.12.008

Millán-Rodríguez, F., Chéchile-Toniolo, G., Salvador-Bayarri, J., Palou, J., Algaba, F., & Vicente-Rodríguez, J. (2000). Primary superficial bladder cancer risk groups according to progression, mortality and recurrence. *The Journal of Urology, 164*(3 Pt 1), 680–684. https://doi.org/10.1016/S0022-5347(05)67280-1

Moroșan, G. C., Moroșan, A.-C., Dobrin, R., Gavril, L. C., Ciobica, A., & Sava, A. (2024). Distribution of astrocytic tumors and brain metastases by anatomical location: A study conducted on 91 patients. *Medical-Surgical Journal – Revista Medico-Chirurgicală a Societății de Medici și Naturaliști din Iași, 128*(3), 577–586. https://doi.org/10.22551/MSJ.2024.03.16

Naspro, R., La Croce, G., Finati, M., Roscigno, M., Pellucchi, F., Sodano, M., Manica, M., Gianatti, A., & Da Pozzo, L. F. (2022). Oncological outcomes of concomitant carcinoma in situ at radical cystectomy in pure urothelial bladder cancer and in histological variants. *Urologic Oncology, 40*(2), 61.e9–61.e19. https://doi.org/10.1016/j.urolonc.2021.07.009

Novac, B., Radu, Z., & Ciobica, A. (2024). Artificial intelligence in urology: New technologies with major potential. *BRAIN – Broad Research in Artificial Intelligence and Neuroscience, 16*(4), 319–324. http://dx.doi.org/10.70594/brain/15.4/21

Pan, J., Hong, G., Zeng, H., Liao, C., Li, H., Yao, Y., Gan, Q., Wang, Y., Wu, S., & Lin, T. (2023). An artificial intelligence model for the pathological diagnosis of invasion depth and histologic grade in bladder cancer. *Journal of Translational Medicine, 21*, 42. https://doi.org/10.1186/s12967-023-03888-z

Park, J. Y., Kim, J., Kim, Y. J., Kim, S. H., An, C. S., Kim, K. G., & Jung, C. K. (2025). Multi-institutional validation of AI models for classifying urothelial neoplasms in digital pathology. *Scientific Reports, 15*, 37215. https://doi.org/10.1038/s41598-025-21096-1

Quhal, F., D'Andrea, D., Soria, F., Moschini, M., Abufaraj, M., Rouprêt, M., Karakiewicz, P. I., Yang, L., Mostafaei, H., Laukhtina, E., Mori, K., Sari Motlagh, R., Rink, M., & Shariat, S. F. (2021). Primary Ta high grade bladder tumors: Determination of the risk of progression. *Urologic Oncology, 39*(2), 132.e7–132.e11. https://doi.org/10.1016/j.urolonc.2020.07.017

Schulze, M., Stotz, N., & Rassweiler, J. (2007). Retrospective analysis of transurethral resection, second-look resection, and long-term chemo-metaphylaxis for superficial bladder cancer: Indications and efficacy of a differentiated approach. *Journal of Endourology, 21*(12), 1533–1541. https://doi.org/10.1089/end.2007.9866

Shariat, S. F., Karakiewicz, P. I., Palapattu, G. S., Lotan, Y., Rogers, C. G., Amiel, G. E., Vazina, A., Gupta, A., Bastian, P. J., Sagalowsky, A. I., Schoenberg, M. P., & Lerner, S. P. (2006). Outcomes of radical cystectomy for transitional cell carcinoma of the bladder: A contemporary series from the Bladder Cancer Research Consortium. *The Journal of Urology, 176*(6 Pt 1), 2414–2422. https://doi.org/10.1016/j.juro.2006.08.004

Sylvester, R. J., van der Meijden, A. P., Oosterlinck, W., Witjes, J. A., Bouffioux, C., Denis, L., Newling, D. W., & Kurth, K. (2006). Predicting recurrence and progression in individual patients with stage Ta T1 bladder cancer using EORTC risk tables: A combined analysis of 2596 patients from seven EORTC trials. *European Urology, 49*(3), 466–477. https://doi.org/10.1016/j.eururo.2005.12.031

van Rhijn, B. W., Burger, M., Lotan, Y., Solsona, E., Stief, C. G., Sylvester, R. J., Witjes, J. A., & Zlotta, A. R. (2009). Recurrence and progression of disease in non–muscle-invasive bladder cancer: From epidemiology to treatment strategy. *European Urology, 56*(3), 430–442. https://doi.org/10.1016/j.eururo.2009.06.028

Witjes, J. A., Lebret, T., Compérat, E. M., Cowan, N. C., De Santis, M., Bruins, H. M., Hernández, V., Espinós, E. L., Dunn, J., Rouanne, M., Neuzillet, Y., Veskimäe, E., van der Heijden, A. G., Gakis, G., & Ribal, M. J. (2017). Updated 2016 EAU guidelines on muscle-invasive and metastatic bladder cancer. *European Urology, 71*(3), 462–475. https://doi.org/10.1016/j.eururo.2016.06.020

Zhang, Y., Rumgay, H., Li, M., Yu, H., Pan, H., & Ni, J. (2023). The global landscape of bladder cancer incidence and mortality in 2020 and projections to 2040. *Journal of Global Health, 13*, 04109. https://doi.org/10.7189/jogh.13.04109